Fraunhofer diffraction of Laguerre–Gaussian beam caused by a dynamic superposed dual-triangular aperture

Li, Xinzhong; Tai, Yuping; Nie, Zhaogang; Wang, Hui; Li, Hehe; Wang, Jingge; Tang, Jie; Wang, Yishan

2015

Fraunhofer diffraction of Laguerre–Gaussian beam caused by a dynamic superposed dual-triangular aperture

Xinzhong Li
Yuping Tai
Zhaogang Nie
Hui Wang
Hehe Li
Jingge Wang
Jie Tang
Yishan Wang

SPIE.

Fraunhofer diffraction of Laguerre–Gaussian beam caused by a dynamic superposed dual-triangular aperture

Xinzhong Li,[a,*] Yuping Tai,[b] Zhaogang Nie,[c] Hui Wang,[a] Hehe Li,[a] Jingge Wang,[a] Jie Tang,[d] and Yishan Wang[d]
[a]Henan University of Science and Technology, School of Physics and Engineering, 263 Kaiyuan Road, Luoyang 471003, China
[b]Henan University of Science and Technology, School of Chemical Engineering and Pharmaceutics, 263 Kaiyuan Road, Luoyang 471003, China
[c]Nanyang Technological University, School of Physical and Mathematical Sciences, 50 Nanyang Avenue, Singapore 637371, Singapore
[d]State Key Laboratory of Transient Optics and Photonics, Chinese Academy of Sciences, 17 Xinxi Road, Xi'an 710119, China

Abstract. We investigate the Fraunhofer diffraction of a Laguerre–Gaussian (LG) beam incident on a dynamic superposed dual-triangular aperture. The evolution of the diffraction pattern from this aperture is analyzed experimentally and theoretically. A special aperture, called the hex-star triangular aperture, demonstrates interesting diffraction patterns. Further, the diffraction properties of integer, half-integer, and fractional orders of topological charges at the Fraunhofer zone are studied by using the hex-star triangular aperture. This study can provide additional information to enhance the understanding of the diffraction properties of the LG beam transmitted through a complex aperture. © 2015 Society of Photo-Optical Instrumentation Engineers (SPIE) [DOI: 10.1117/1.OE.54.12.123113]

1 Introduction

Optical vortices have attracted considerable attention since the seminal paper of phase singularities was published by Nye and Berry.[1] Optical vortices are applied in different research fields such as quantum information communication,[2,3] micro-particle manipulation,[4–6] light beam knots,[7,8] and image processing[9–13] among others.[14–22] An optical vortex has a spiral phase of $\exp(im\phi)$ and carries an orbital angular momentum (OAM) of $m\hbar$, where m is the topological charge (TC).

The diffraction properties that can be used to determine the order of the TC of the vortex beam have recently attracted considerable attention. Based on the properties of far-field diffraction (Fraunhofer zone) of an aperture, many methods to measure the TC of an optical vortex were proposed. Most of these methods were based on counting the number of diffracted fringes or spots.[23–28] Recently, Hickmann et al. developed an equilateral-triangular aperture, which easily measures the magnitude and sign of the TCs.[23,24] This method is suitable for measuring both cw and femtosecond vortices because of the simplicity and reliability of the aperture.[25] This method is also applicable for supercontinuum vortices when spatial dispersion is compensated.[26] Furthermore, this method can be used to determine the TC of an electron vortex beam.[27]

Triangular apertures have extended versatility because they can observe the birth of a vortex at the Fraunhofer zone. The birth of a vortex is observed in different conditions when the fractional part of noninteger TCs is more[28] or less[29] than those of half-integer TCs. Moreover, the triangular aperture is used for shaping the spatial intensity profile of vortex beams in a controlled manner.[30] Deformed triangular apertures, such as an annular triangular aperture[31] and triangular multipoint plate,[32] effectively determine the order of TCs and their signs. However, there is a little literature on the

evolution of diffraction patterns from a dynamic complex aperture, which is important for understanding the diffraction properties of the vortex beam. In addition, the properties of the Fraunhofer diffraction of deformed triangular apertures should be further investigated to expand the application of these apertures.

In order to visualize the diffraction properties of a Laguerre–Gaussian (LG) beam transmitted through a complex aperture, we studied the Fraunhofer diffraction of the LG vortex beam incident on a dynamic superposed dual-triangular aperture. First, a change in the diffraction pattern of a certain LG beam with respect to the aperture deformation was studied. Then, a distinctive aperture, named a hex-star triangular aperture, was constructed. By using this particular aperture, the diffraction patterns of the LG beam of the different orders (i.e., integer, half-integer, and fractional number) of the TCs were studied in detail. Furthermore, surprising phenomena were observed.

2 Theoretical Background

Initially, a changing superposed dual-triangular aperture, which consists of two equilateral triangles with a common center and inverse placement directions, was constructed. The overlapped area was blocked. Figure 1 shows the schematic of the aperture. The centers of the two triangles are located at the origin of the coordinates on the $x_0 y_0$ plane. The transmission function of the upper-triangular aperture (t_1) is given by

$$t_1(x_0, y_0) = \begin{cases} 1, & \left[-\frac{a}{2} \le x_0 \le 0, 0 \le y_0 \le (x_0 + \frac{a}{2}) \cdot \sqrt{3}\right] \\ & \text{and} \left[0 \le x_0 \le \frac{a}{2}, 0 \le y_0 \le (\frac{a}{2} - x_0) \cdot \sqrt{3}\right], \\ 0, & \text{elsewhere} \end{cases}$$

(1)

*Address all correspondence to: Xinzhong Li, E-mail: lixinzhong7922@163.com
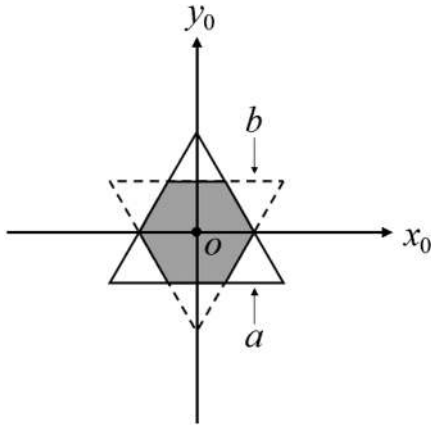
Fig. 1 Schematic of a changing superposed dual-triangular aperture.

where a is the side length of the triangle. The lower-triangular aperture (t_2) with the side length b, represented by a dotted line in Fig. 1, can be obtained by flipping t_1 upside down [denoted by flipud $(\dots)$]

$$t_2(x_0, y_0) = \text{flipud}[t_1(x_0, y_0)], \qquad (2)$$

where the side length of t_2 is denoted by b instead of a. Thus, the changing superposed dual-triangular aperture is constructed, and its transmission function is given by

$$t(x_0, y_0) = [t_1(x_0, y_0) \cup t_2(x_0, y_0)][t_1(x_0, y_0) \cap t_2(x_0, y_0)]. \qquad (3)$$

In this case, a fixed value is assigned to a, whereas the value of b is varied to obtain differently shaped apertures.

The LG beam is particularly interesting because it is usually used to characterize the vortex beam that has optical vortices and carries OAM. The LG beam has a helical wave front with phase singularity at the center of the beam. The electric field amplitude of the LG beam at the beam waist is written in cylindrical coordinates (r, θ, z) as

$$LG_p^l(r, \theta, z = 0) = A \cdot (2r^2/w_0^2)^{|l|/2} \cdot L_p^{|l|}(2r^2/w_0^2) \\ \cdot \exp(-r^2/w_0^2) \exp(il\theta), \qquad (4)$$

where $L_p^{|l|}$ is the generalized Laguerre polynomial and w_0 is the waist size of the beam. LG beams are described by l and p indices representing the azimuthal and radial mode numbers, respectively. The azimuthal mode index l is an integer that represents the order of the TC of a vortex beam. The radial mode index p determines the number of bright rings that surround the central dark spot $p + 1$.

Equation (4) can be simplified to

$$LG_0^l(r, \theta, z = 0) = \left(\sqrt{2}r/w_0\right)^{|l|} \exp(-r^2/w_0^2) \exp(il\theta) \qquad (5)$$

for the LG beams with $p = 0$ and $A = 1$.

In our study, we consider an incident beam to have an exponential phase $\exp[i(l + \varepsilon)\theta]$, where ε is a fraction within the interval of 0 to 1. Thus, the incident beam of Eq. (5) is rewritten as
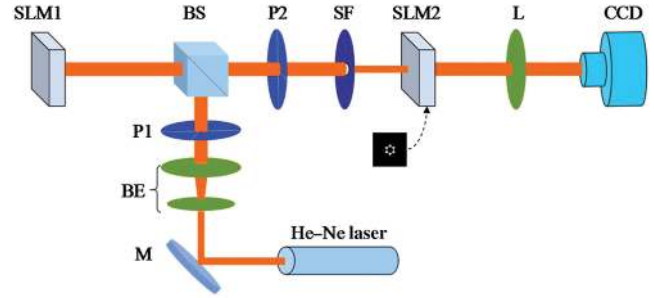
Fig. 2 Experimental schematic of recording the Fraunhofer diffraction patterns. BE, beam expander; BS, beam splitter; M, mirror; L, lens; P1 and P2, polarizers; SF, spatial filter; SLM1 and SLM2, spatial light modulators.

$$U_0^m(r, \theta, z = 0) = \left(\sqrt{2}r/w_0\right)^{|m|} \exp(-r^2/w_0^2) \exp(im\theta), \qquad (6)$$

where $m = l + \varepsilon$, which represents the TC.

When a modified LG beam represented by Eq. (6) illuminates the center of the dynamically superposed dual-triangular aperture perpendicular to the observation plane of the Fraunhofer zone, the complex amplitude of the wave field can be calculated by using the Fresnel–Kirchhoff integral

$$U(x, y, z \to \infty) = \frac{\exp(ikz)}{i\lambda z} \exp\left[\frac{ik}{2z}(x^2 + y^2)\right] \\ \times \iint_\infty U_0^m(x_0, y_0) t(x_0, y_0) \\ \times \exp\left[-i\frac{2\pi}{\lambda z}(xx_0 + yy_0)\right] dx_0 \, dy_0, \qquad (7)$$

where λ is the wavelength of the incident beam and k is the wave number. In this case, the transverse coordinates on the aperture plane are $(x_0, y_0) = (r, \theta)$ in either Cartesian or cylindrical polar coordinates, and the modified LG beam function is written as $LG(x, y) = LG(r, \theta)$.

3 Experimental Setup

The experimental setup is shown in Fig. 2. A helium–neon laser with a wavelength of 632.8 nm and power of 2 mW is used as the light source. After reflection by a mirror, the Gaussian beam passed through a beam expander that allowed us to obtain a collimated beam with a planar wavefront. Then the collimated beam illuminated a reflective phase-only spatial light modulator (SLM1).
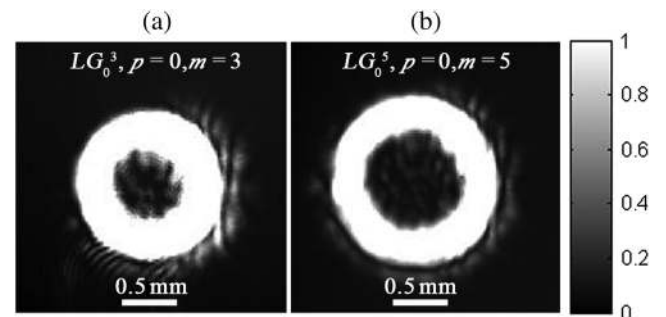
Fig. 3 Intensity images of the Laguerre–Gaussian (LG) beam [(a) LG_0^3 and (b) LG_0^5] generated by the SLM1.
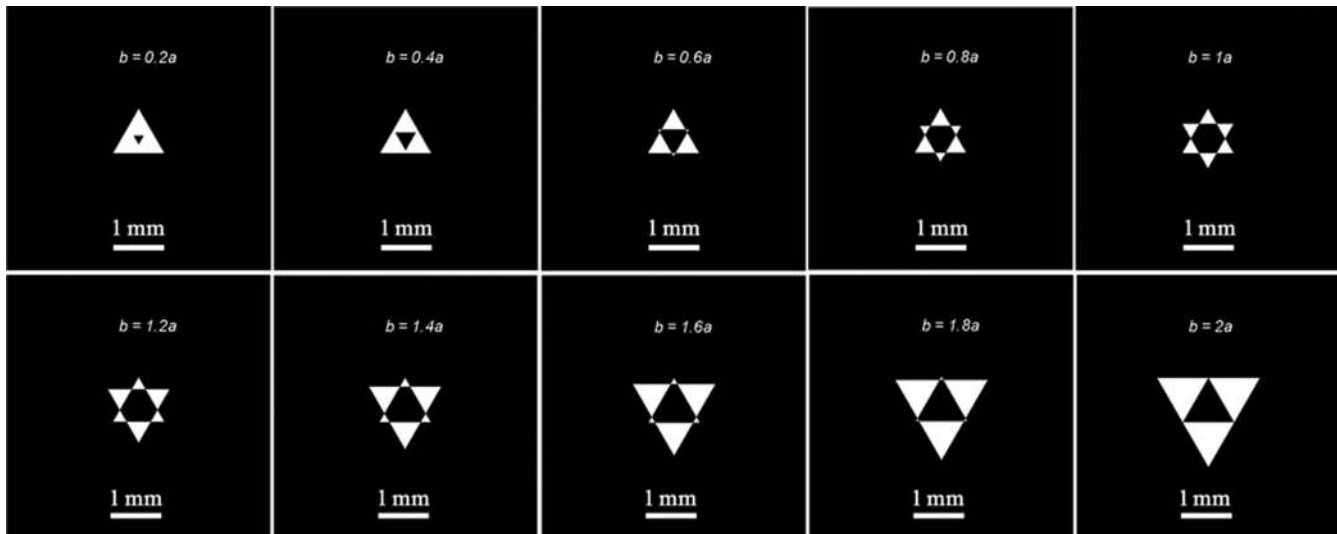
Fig. 4 Aperture structure changes with edge length of a lower-equilateral triangle when b is increased from 0.2a to 2a in. increments of 0.2a. The change process of the aperture structure with respect to the increase of b from 0.2a to 2a in. increments of 0.2a is demonstrated in Video 1. (Video 1, WMV, 494 KB) [URL: http://dx.doi.org/10.1117/1.OE.54.12.123113.1].
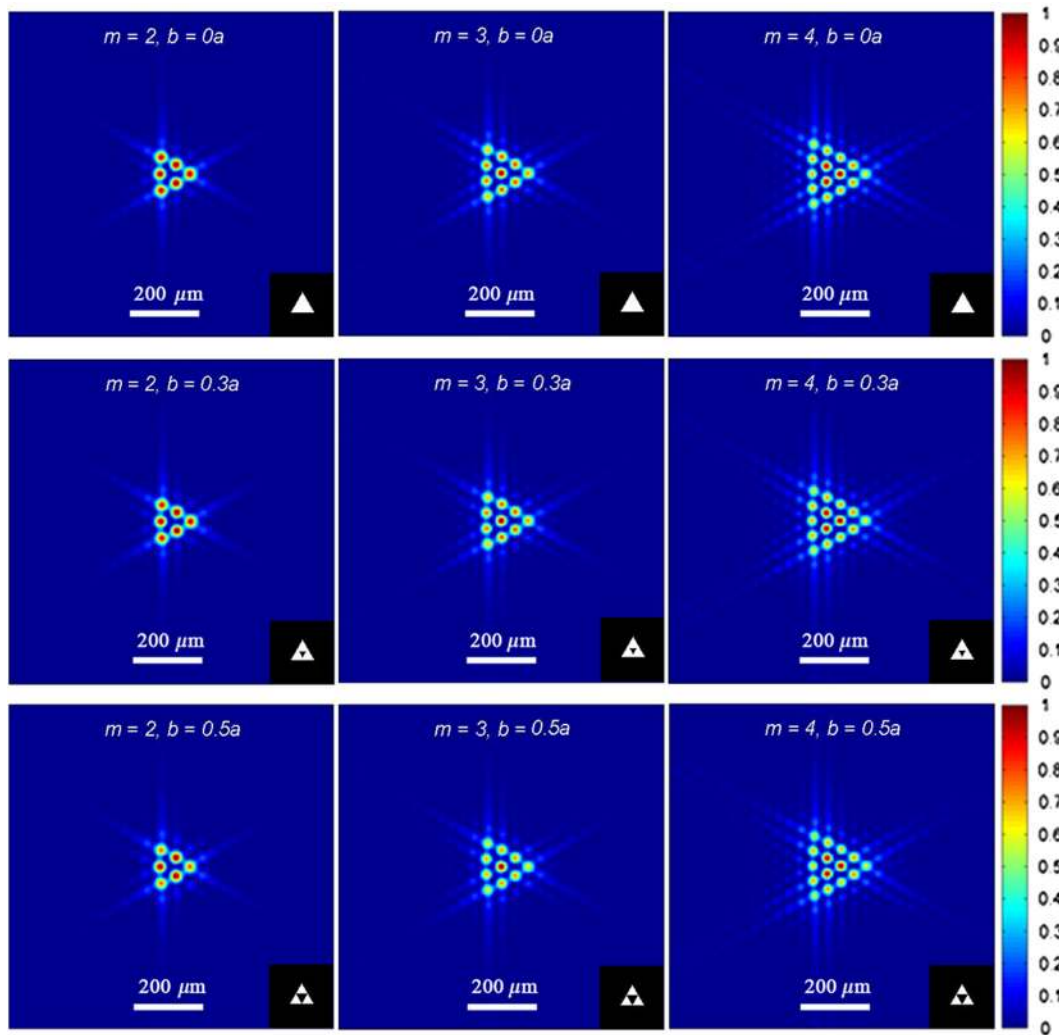
Fig. 5 Diffraction patterns at the Fraunhofer zone with different aperture structures (numerical simulation results). Vertical direction: left panel, $m = 2$; middle panel, $m = 3$; and right panel, $m = 4$. Horizontal direction: upper panel, $b = 0$; middle panel, $b = 0.3a$; and lower panel, $b = 0.5a$. The insets show the aperture.
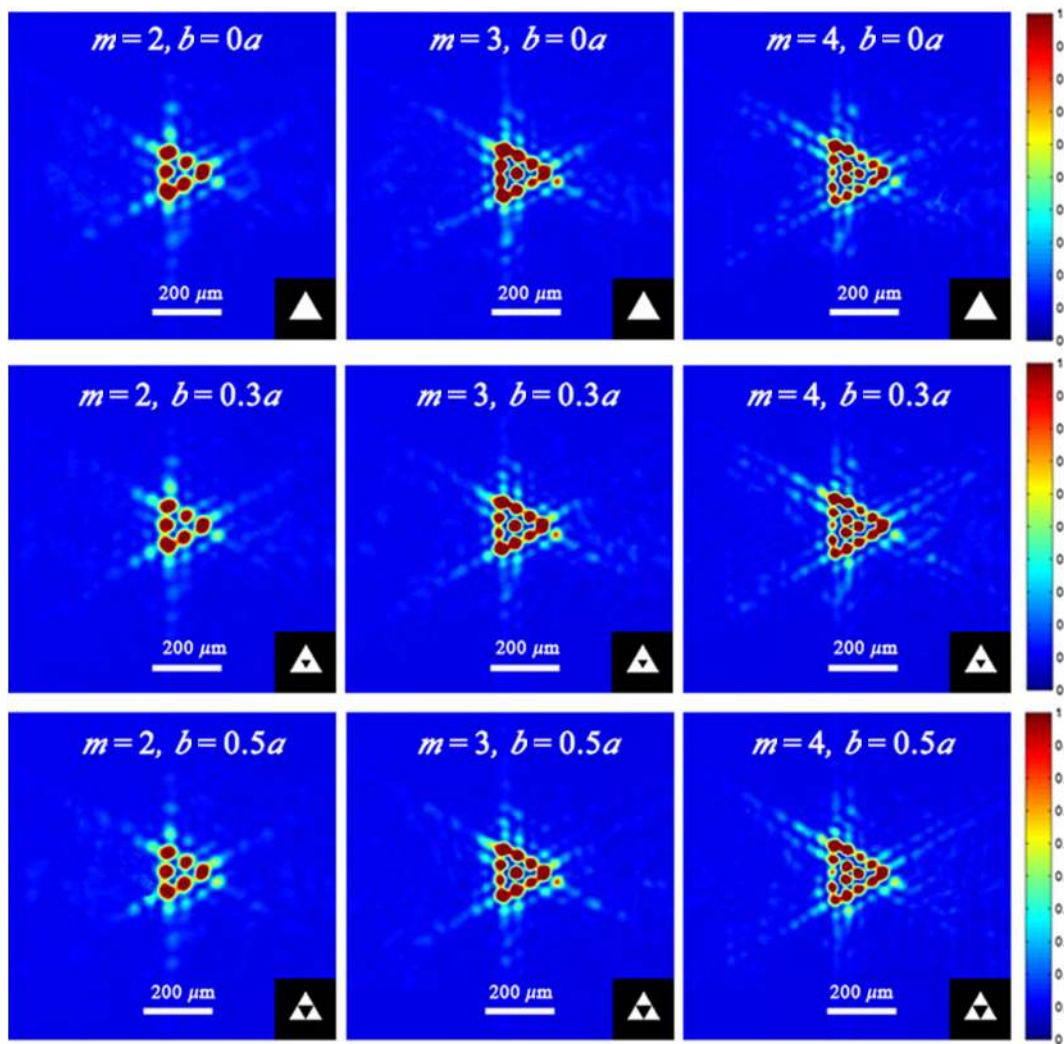
Fig. 6 Experimental diffraction patterns at the Fraunhofer zone with different aperture structures. Vertical direction: left panel, $m = 2$; middle panel, $m = 3$; and right panel, $m = 4$. Horizontal direction: upper panel, $b = 0$; middle panel, $b = 0.3a$; and lower panel, $b = 0.5a$. The insets show the aperture.

The LG beam was obtained by using a spatial filter to select the first-diffraction order beam from SLM1. A second spatial light modulator (SLM2) was used as the dynamic superposed dual-triangular aperture that allowed us to flexibly change the geometry of the aperture by using dedicated LabVIEW software. Therefore, we were able to change the size of the aperture to the size of the LG beam when changing the index. A CCD camera (Basler acA1600-20 gm/gc, pixel size: $4.4~\mu\mathrm{m} \times 4.4~\mu\mathrm{m}$, resolution: 1626×1236 pixels) was used to record and save the interference patterns on a computer. The CCD camera was fixed on a motorized stage driven by a stepping motor, which was used to locate the Fourier plane.

Figures 3(a) and 3(b) show two of the experimental intensity images of the LG beam [(a) LG_0^3 and (b) LG_0^5]. Obviously, as the TC of LG beam is increased, the radius of the LG beam also increases. As the TCs increased from 1 to 10, the radii of the LG beams increased from 0.3 to 2.5 mm, approximately.

4 Results and Discussions

The Fraunhofer diffraction patterns obtained as a result of diffraction of the LG vortex beams incident on the dynamic

superposed dual-triangular aperture were determined by solving Eq. (7). The edge length of the lower-equilateral triangle b was changed from 0 to $2a$, where a was fixed as 3.0 mm. This procedure was performed to study the diffraction properties of different aperture structures. Figure 4 shows the aperture structure formed by increasing b from $0.2a$ to $2a$. Meanwhile, the dynamic process of the aperture modification is demonstrated in Video 1 with respect to the increase of b from 0 to $2a$ in. increments of $0.01a$. When $0 \leq b \leq 0.5a$, the aperture changed to an upper-equilateral-triangular aperture with an obstacle in the center. When $0.5 < b < 2a$, the aperture consisted of six equilateral triangles, and when $b \geq 2a$, the aperture changed to a lower-equilateral-triangular aperture with an obstacle in the center.

The diffraction properties of the LG beam varied when b was increased in the given azimuthal indices. When b was 0 to $0.5a$, the TC could be determined by using the equation $m = N - 1$, where N is the number of spots on any edge of the triangle in the diffraction patterns. Moreover, in cases when the TC became its opposite number, the diffraction triangular pattern was rotated 180 deg in comparison to the previous one. These results were found to be consistent
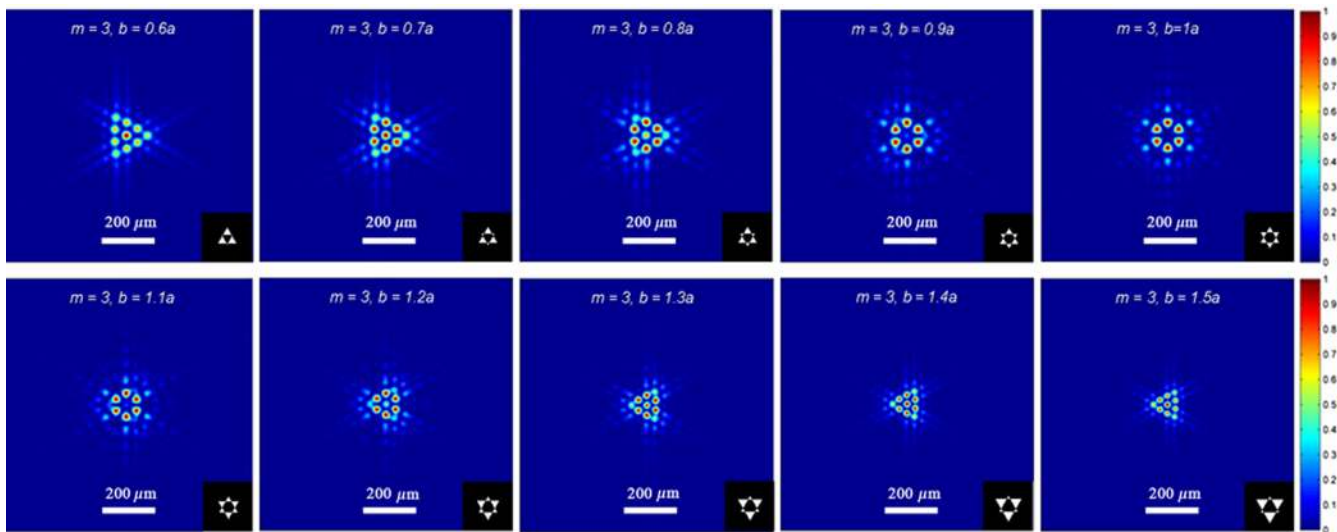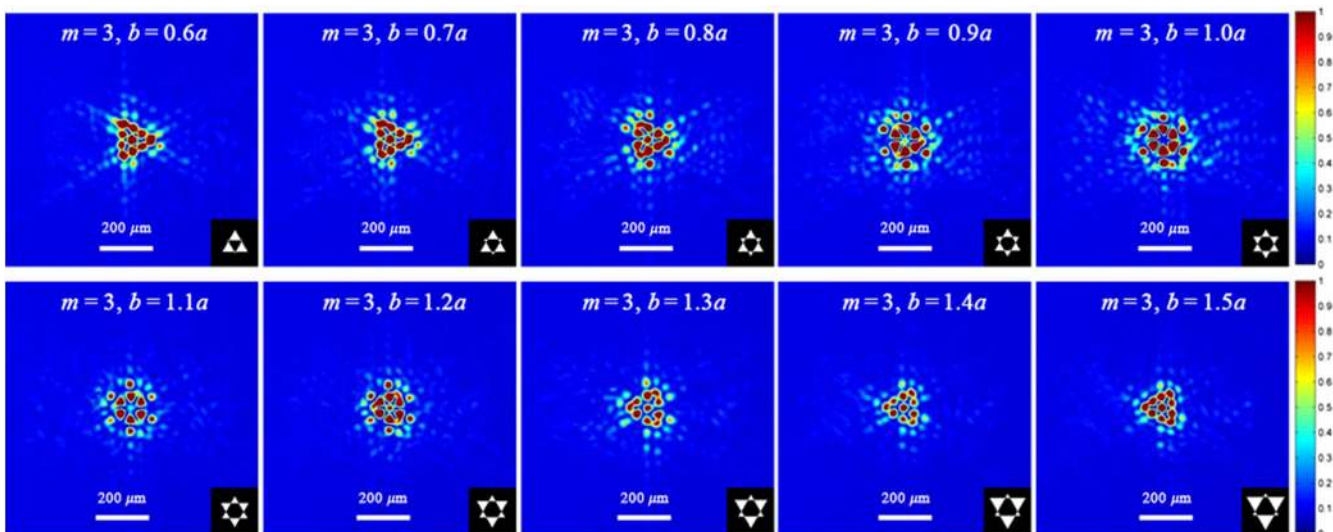
Fig. 7 Diffraction pattern change when *b* is increased from 0.6*a* to 1.5*a* in. increments of 0.1*a* (numerical simulation results). The insets show the diffraction apertures. Videos 2–4 demonstrate the detailed change in the diffraction patterns of *m* = 3, 4, and 5 when *b* is increased from 0.6*a* to 1.5*a* in. increments of 0.01*a*. (Videos 2–4, WMV, 444 KB; WMV, 606 KB; WMV, 759 KB) [URL: http://dx.doi.org/10.1117/1. OE.54.12.123113.2]; [URL: http://dx.doi.org/10.1117/1.OE.54.12.123113.3]; [URL: http://dx.doi.org/ 10.1117/1.OE.54.12.123113.4].

with the results of the previous study on diffraction using the triangular aperture.[22]

Figures 5 and 6 show the theoretical and experimental intensity distributions of the diffracted wave field when $m = 2$, 3, and 4 in different aperture conditions of $b = 0, 0.3a$, and $0.5a$, respectively. We can see that the experimental results are in good agreement with the theoretical results. The triangle of the diffraction pattern was rotated 30 deg with respect to the aperture (insets) because of the interference of edge waves.[33] The intensity indicated by the bright spots increased with the increase of the size of the lower triangle. Compared with the theoretical results, the distribution of the bright spots in the experimental diffraction patterns was uneven because of the asymmetric optical path. However, the magnitude and sign of the TC could be measured by the rule mentioned above ($m = N - 1$).

These results indicated that the method of triangular aperture diffraction is reliable for measuring the TC of the LG beam. This method is useful to determine the TCs of LG beam up to $m = 7$. It is very difficult to arrange the experimental elements for higher-order TCs' measurements.[23] Compared to interferometric methods of measuring the TC of the LG beams,[33] this method eliminated the effect of obstacles and parasitic interference. Simultaneously, the experimental setup of this method is simple and the perfect diffraction patterns are easily obtained.

The upper triangle was cut into three smaller upper triangles, and the center was completely shadowed when $b = 0.5a$. When $0.5a < b < 1.5a$, the aperture became a six-triangular aperture, which consisted of three same-sized upper-equilateral triangles and three same-sized lower-equilateral triangles. These six triangles were connected by a shaded hexagon.

Fig. 8 Experimental diffraction patterns change when *b* is increased from 0.6*a* to 1.5*a* in. increments of 0.1*a*. The insets are the diffraction apertures.
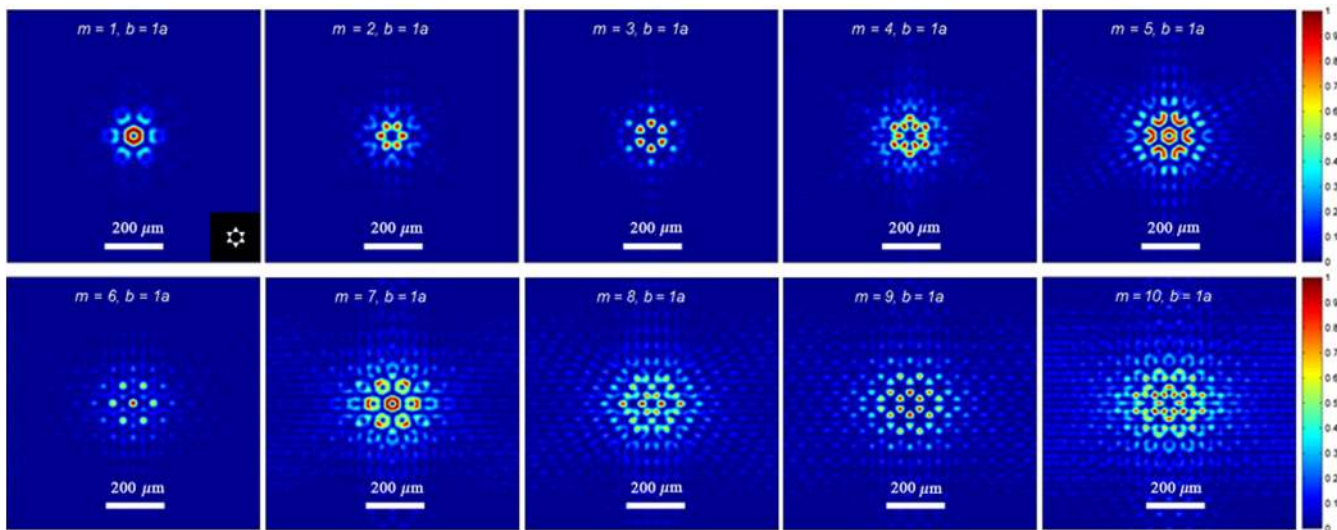
Fig. 9 Diffraction patterns of different integer topological charges (TCs) vortex beam at the Fraunhofer zone for m from 1 to 10 (numerical simulation results). The inset shows the diffraction aperture when $b = 1a$.
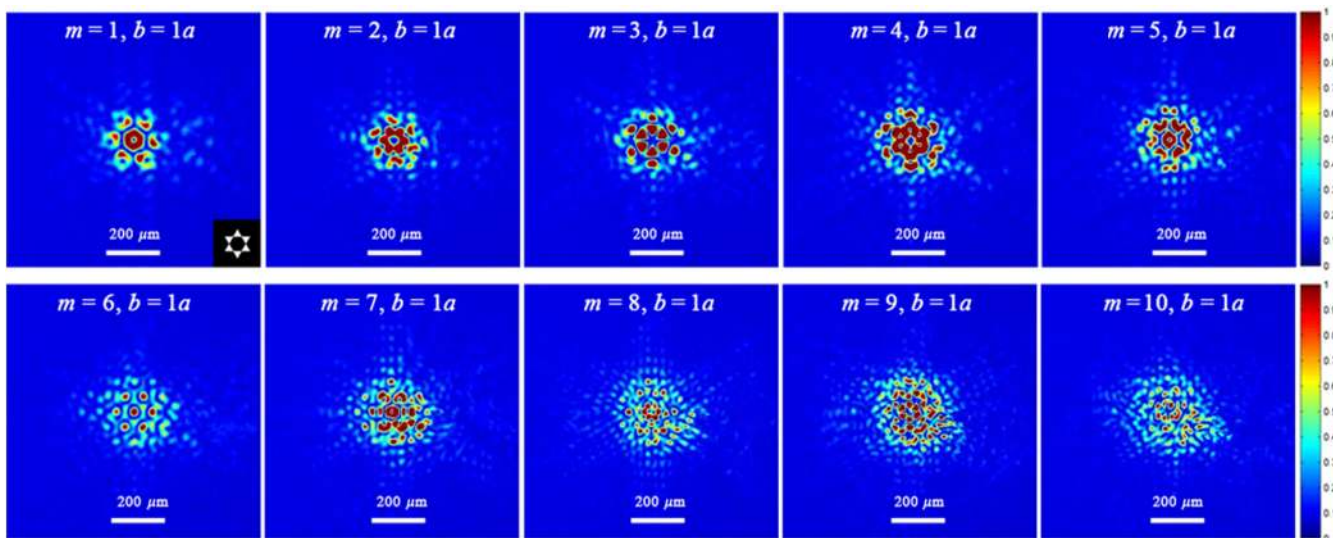
Fig. 10 Experimental diffraction patterns of different integer TCs vortex beam at the Fraunhofer zone for m from 1 to 10. The inset shows the diffraction aperture when $b = 1a$.

The diffraction patterns exhibited interesting changes during this process. Figures 7 and 8 show the theoretical and experimental changes in the diffraction patterns, respectively, when b is increased from $0.6a$ to $1.5a$ in. increments of $0.1a$. The experimental results are in good agreement with the theoretical results. Both results showed that the bright spots of the triangle gradually formed a hexagon when b was increased from $0.6a$ to $1.0a$. The structures of the diffraction patterns changed to another triangular distribution when b was increased from $1.0a$ to $1.5a$. However, the triangular diffraction pattern rotated 60 deg clockwise compared with the previous one. The physical insight is that, in this case, the diffraction effect is determined from the diffraction of three upper-equilateral triangles to the lower ones.

The diffraction pattern of an optical field from an aperture was the result of the interference between edge waves. In this

case, each diffraction pattern was formed by three sets of interfering parallel lines because the sides of these six triangles were either collinear or parallel. The detailed change in the diffraction patterns of $m = 3$, 4, and 5 when b is increased from $0.6a$ to $1.5a$ in. increments of $0.01a$ is demonstrated in Videos 2–4 (numerical simulation results).

The diffraction patterns had similar shapes and became smaller when b was further increased ($b > 1.5a$) because the aperture increased simultaneously with b. The six triangles of the aperture were similar-sized when $b = 1a$, and the whole aperture looked like a hex star. In this case, diffraction by the aperture demonstrated high symmetry. The diffraction properties of the hex-star triangular aperture with different TCs were studied in detail.

Figures 9 and 10 show the theoretical and experimental diffraction patterns of different integer-order TCs at the
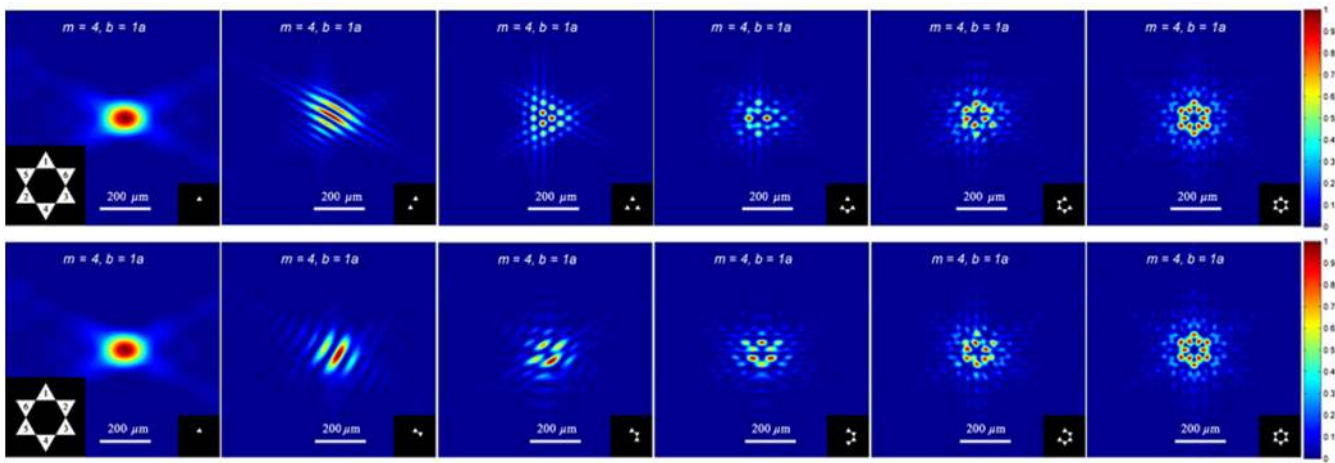
Fig. 11 Diffraction patterns of partial aperture of the hex-star triangular aperture when $m = 4$ and $b = 1a$ (numerical simulation results). The upper and lower panels illustrate the diffraction patterns at different moments of the formation processes of the aperture. The large insets represent the formation process of the aperture (numbers are in the order of appearance), and the small insets are the diffraction apertures.
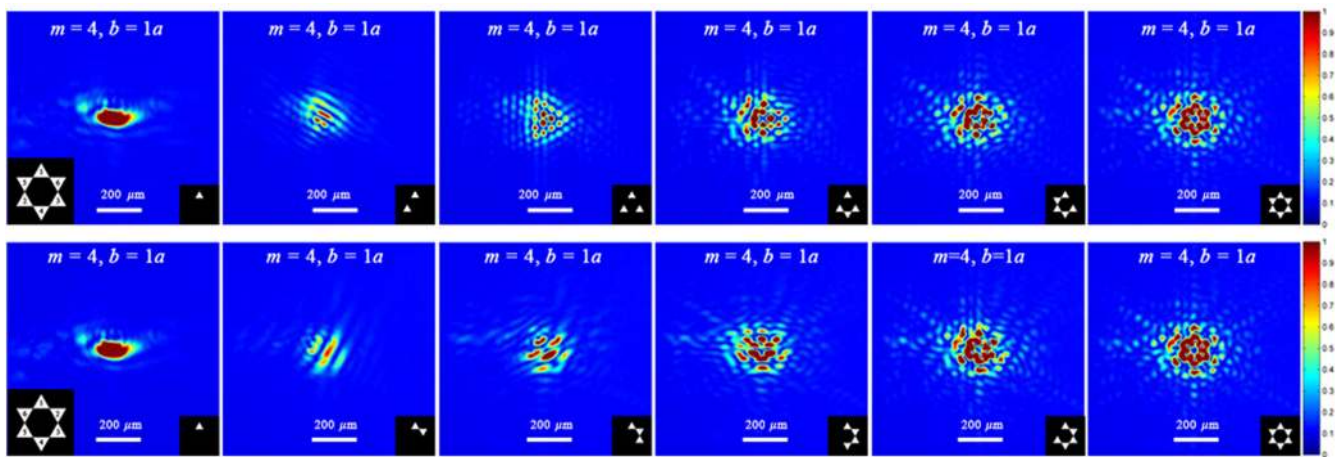
Fig. 12 Experimental diffraction patterns of partial aperture of the hex-star triangular aperture when $m = 4$ and $b = 1a$ under the same condition described in the caption of Fig. 11.
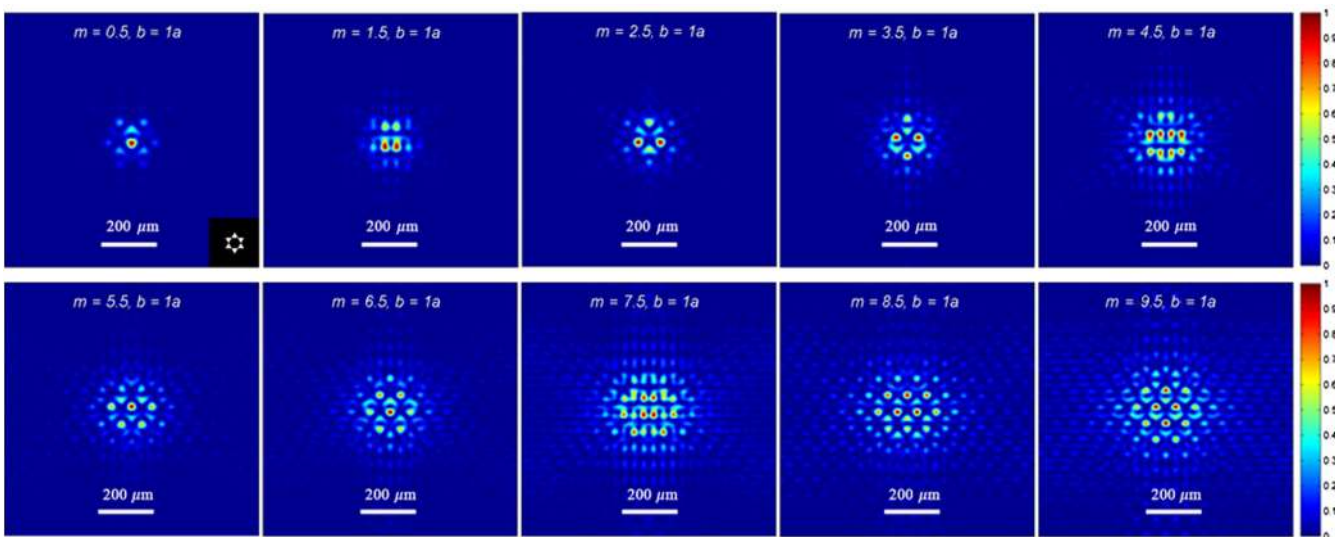
Fig. 13 Diffraction patterns of half-integer TCs at the Fraunhofer plane (numerical simulation results). The inset shows the diffraction aperture when $b = 1a$.
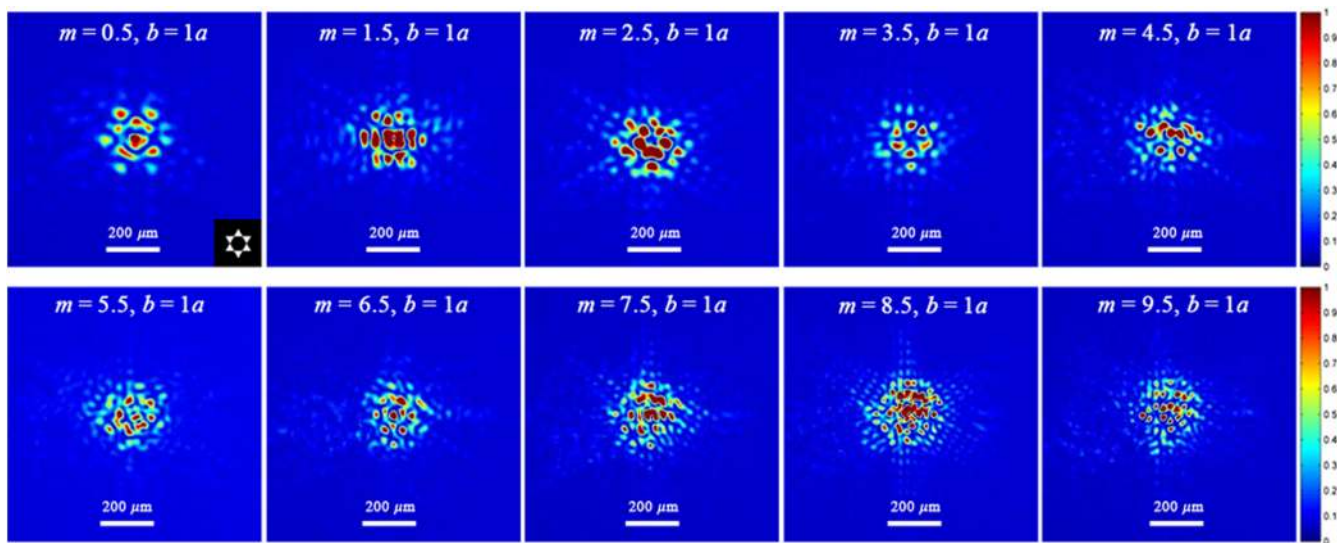
Fig. 14 Experimental diffraction patterns of half-integer TCs at the Fraunhofer plane. The inset shows the diffraction aperture when $b = 1a$.

Fraunhofer zone when m ranges from 1 to 10 and the LG beam illuminates the hex-star-triangular aperture. We can see that the diffraction patterns become more complex and the diffraction effect becomes stronger when m is increased. In this case, the diffraction patterns are related to the shape of the aperture and incident beam. The radius of the doughnut LG beam increased with the TC. Thus, the aperture became relatively small, leading to a strong diffraction effect. The interfered patterns became more complex when the number of spots on the outside edge of the diffracted patterns was increased by increasing m. Moreover, the symmetry of the diffraction patterns of an odd TC value was higher than that of an even TC value, which is possibly due to the even number of small triangles in the hex-star aperture. The diffraction patterns obtained by experiments gradually deviated from the theoretical patterns when the TC increased,

which was due to the complex patterns resulting in significant adjustments.

Each diffraction pattern was considered as interference caused by the complex amplitudes of the diffraction field of each small triangle of the hex-star aperture. The six triangles of the hex-star aperture were placed one-by-one to calculate the diffraction intensity. This process was performed to study the formation process of the diffraction patterns from the hex-star aperture. Figures 11 and 12 show the theoretical and experimental diffraction patterns from the partial aperture at two different processes of the construction of the aperture when $m = 4$ and $b = 1a$, respectively. It is clearly shown that the experimental results are consistent with the numerical simulation results. The diffraction patterns were obviously different for different processes of the combination of the six triangles. Meanwhile, the symmetry axis of
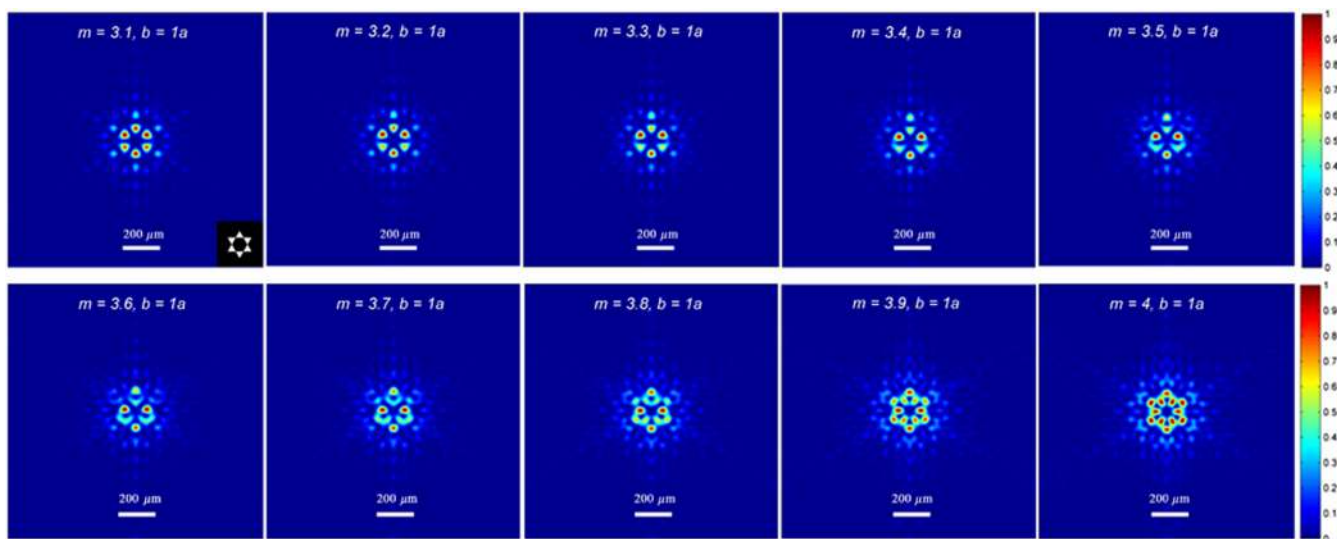
Fig. 15 Evolution of diffraction patterns of different fractional TCs vortex beam when m increases from 3.1 to 4 in. increments of 0.1 and $b = 1a$ (numerical simulation results). Video 5 shows the change of the TCs from 0 to 10 in. increments of 0.1. (Video 5, WMV, 1.03 MB) [URL: http://dx.doi.org/10.1117/1.OE.54.12.123113.5].
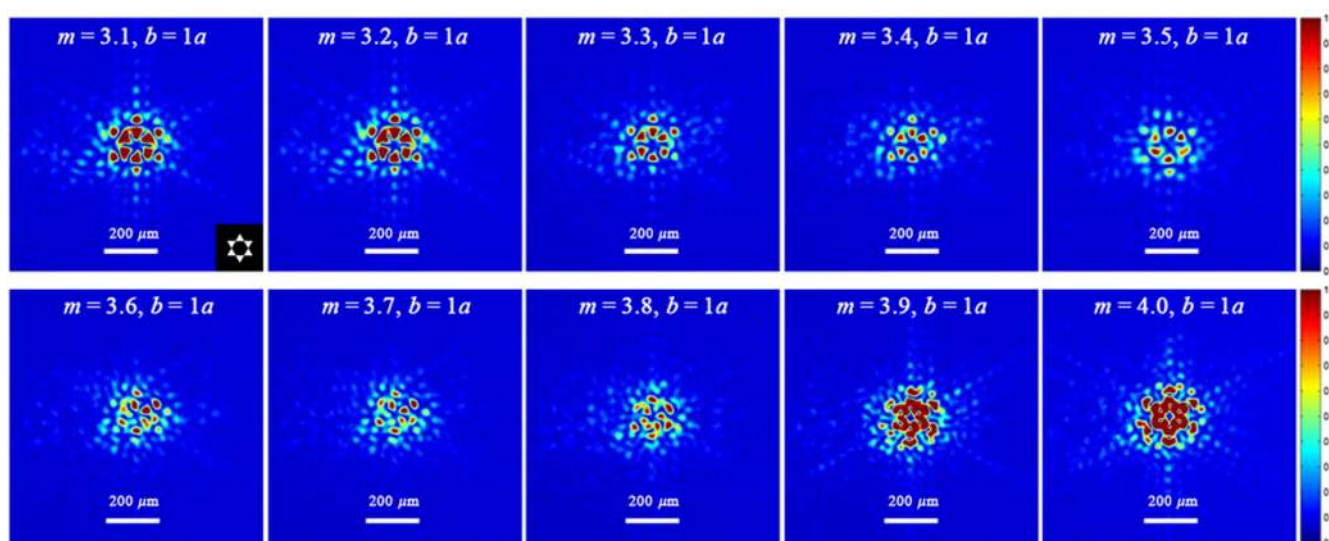
Fig. 16 Evolution of diffraction patterns of different fractional TCs vortex beam when m increases from 3.1 to 4 in. increments of 0.1 and $b = 1a$ (experimental results).

the diffraction pattern was perpendicular to that of the partial aperture.

The triangular spots in the diffraction pattern do not appear when the center of a single aperture does not overlap with the LG beam center, as shown in the first columns of Figs. 11 and 12. However, if three triangles were arranged at the center of the incident LG vortex beam, the diffraction patterns were used to determine the TC by counting the number of external points of the triangular lattice (row 1, column 3 in Figs. 11 and 12).

Figures 11 and 12 show the formation process of the hex-star diffraction, which deepens our understanding of the diffraction properties of the LG beam. In order to observe the diffraction patterns of noninteger vortex beams, the theoretical and experimental diffraction intensity distributions of half-integer orders are illustrated in Figs. 13 and 14, respectively. Comparing the diffraction patterns of the adjacent integer TCs, we can see that the symmetry of the diffraction patterns of half-integer TCs disappears and a vertical symmetry appears, as shown in Fig. 13. This phenomenon was caused by the axial symmetry of the half-integer vortex beam, which had a radial line of low intensity.[34,35] Because of the influence of the stray light, the symmetry of the experimental diffraction patterns gradually disappeared.

Finally, the evolution of the diffraction patterns of the other fractional TCs from the hex-star aperture was investigated. Figures 15 and 16 show the theoretical and experimental diffraction patterns, respectively, when m was increased from 3 to 4 in. increments of 0.1. The diffraction patterns also had bilateral symmetry, and only a slight change between the adjacent patterns was observed. Figures 15 shows the process of evolution of the diffraction patterns from circular symmetry to axial symmetry and again to circular symmetry, corresponding to the evolution of the intensity distribution of the LG vortex beam. To visualize the transformation, a movie (i.e., Video 5) is used to illustrate the change in vortex charge from 0 to 10 in. increments of 0.1 (numerical simulation results). However, Fig. 16 shows that the experimental results are found to be

inconsistent with the theoretical results since the adjustment becomes more significant for a fractional TCs vortex beam.

Moreover, only the LG_0^m vortex beam was investigated in this study. Further studies should be conducted for radial mode numbers $p \neq 0$. The spatial relationship between the LG beam waist and aperture should be considered.[36]

5 Conclusion

In summary, a dynamic superposed dual-triangular aperture was constructed, and its Fraunhofer diffraction evolution was investigated in detail when an LG vortex beam was transmitted through it. The diffraction properties of integer, half-integer, and fractional TCs at the Fraunhofer zone were studied in detail by using the hex-star aperture. The experimental results were found to be consistent with the numerical simulation results. Thus, our study contributes to understanding the properties of the LG vortex beam. Further, interesting images as a result of Fraunhofer diffraction of the vortex beam having different TCs incident on the hex-star triangular aperture were obtained. This method can be used in various applications such as shaping the spatial intensity of an LG vortex beam, laser shows, and optical tweezers.

References

1. J. F. Nye and M. V. Berry, "Dislocations in wave trains," *Proc. R. Soc. A: Math. Phys. Eng. Sci.* **336**, 165–190 (1974).
2. G. Molina-Terriza, J. P. Torres, and L. Torner, "Twisted photons," *Nat. Phys.* **3**, 305–310 (2007).
3. N. Bozinovic et al., "Terabit-scale orbital angular momentum mode division multiplexing in fibers," *Science* **340**, 1545–1548 (2013).
4. D. G. Grier, "A revolution in optical manipulation," *Nature* **424**, 810–816 (2003).

5. S. Tao et al., "Fractional optical vortex beam induced rotation of particles," *Opt. Express* **13**, 7726–7731 (2005).
6. J. Ng, Z. Lin, and C. T. Chan, "Theory of optical trapping by an optical vortex beam," *Phys. Rev. Lett.* **104**, 103601 (2010).
7. J. Leach et al., "Laser beams: knotted threads of darkness," *Nature* **432**, 165–165 (2004).
8. M. R. Dennis et al., "Isolated optical vortex knots," *Nat. Phys.* **6**, 118–121 (2010).
9. K. Crabtree, J. A. Davis, and I. Moreno, "Optical processing with vortex-producing lenses," *Appl. Opt.* **43**, 1360–1367 (2004).
10. M. K. Sharma, J. Joseph, and P. Senthilkumaran, "Selective edge enhancement using anisotropic vortex filter," *Appl. Opt.* **50**, 5279–5286 (2011).
11. Y. Pan et al., "Edge extraction using a time-varying vortex beam in incoherent digital holography," *Opt. Lett.* **39**, 4176–4179 (2014).
12. X. Z. Li et al., "Digital speckle correlation method based on phase vortices," *Opt. Eng.* **51**, 077004 (2012).
13. X. Li et al., "Characterization of dynamic random process using optical vortex metrology," *Appl. Phys. B* **116**, 901–909 (2014).
14. L. Ge et al., "Stability of elliptic vortex solitons in anisotropic nonlocal media," *Chin. Opt. Lett.* **12**, 121901 (2014).
15. Z. Fang et al., "Simple Nd:YAG laser generates vector and vortex beam," *Chin. Opt. Lett.* **13**, 031405 (2015).
16. V. P. Aksenov and V. V. Kolosov, "Scintillations of optical vortex in randomly inhomogeneous medium," *Photonics Res.* **3**, 44–47 (2015).
17. P. Chen et al., "Arbitrary and reconfigurable optical vortex generation: a high-efficiency technique using director-varying liquid crystal fork gratings," *Photonics Res.* **3**, 133–139 (2015).
18. Y. Yang et al., "Generation and propagation of an anomalous vortex beam," *Opt. Lett.* **38**, 5418–5421 (2013).
19. Y. Yang et al., "Autocorrelation properties of fully coherent beam with and without orbital angular momentum," *Opt. Express* **22**, 2925–2932 (2014).
20. Y. Yang, M. Mazilu, and K. Dholakia, "Measuring the orbital angular momentum of partially coherent optical vortices through singularities in their cross-spectral density functions," *Opt. Lett.* **37**, 4949–4951 (2012).
21. Y. Yuanjie et al., "Effect of the radial and azimuthal mode indices of a partially coherent vortex field upon a spatial correlation singularity," *New J. Phys.* **15**, 113053 (2013).
22. X. Li et al., "Propagation properties of optical vortices in random speckle field based on Fresnel diffraction scheme," *Opt. Commun.* **287**, 6–11 (2013).
23. J. M. Hickmann et al., "Unveiling a truncated optical lattice associated with a triangular aperture using light's orbital angular momentum," *Phys. Rev. Lett.* **105**, 053904 (2010).
24. L. Clark et al., "Quantitative measurement of orbital angular momentum in electron microscopy," *Phys. Rev. A* **89**, 053818 (2014).
25. L. E. E. de Araujo and M. E. Anderson, "Measuring vortex charge with a triangular aperture," *Opt. Lett.* **36**, 787–789 (2011).
26. M. E. Anderson et al., "Measuring the topological charge of ultra-broadband, optical-vortex beams with a triangular aperture," *J. Opt. Soc. Am. B* **29**, 1968–1976 (2012).
27. G. Guzzinati et al., "Measuring the orbital angular momentum of electron beams," *Phys. Rev. A* **89**, 025803 (2014).
28. A. Mourka et al., "Visualization of the birth of an optical vortex using diffraction from a triangular aperture," *Opt. Express* **19**, 5760–5771 (2011).
29. A. J. Jesus-Silva, E. J. S. Fonseca, and J. M. Hickmann, "Study of the birth of a vortex at Fraunhofer zone," *Opt. Lett.* **37**, 4552–4554 (2012).
30. A. M. Amaral, E. L. Falcão-Filho, and C. B. de Araújo, "Shaping optical beams with topological charge," *Opt. Lett.* **38**, 1579–1581 (2013).
31. Y. Liu et al., "Detecting the topological charge of vortex beams using an annular triangle aperture," *Opt. Laser Technol.* **43**, 1233–1236 (2011).
32. Y. Liu, J. Pu, and B. Lü, "Method for exploring the orbital angular momentum of an optical vortex beam with a triangular multipoint plate," *Appl. Opt.* **50**, 4844–4847 (2011).
33. X. Li et al., "Measuring the fractional topological charge of LG beams by using interference intensity analysis," *Opt. Commun.* **334**, 235–239 (2015).
34. M. V. Berry, "Optical vortices evolving from helicoidal integer and fractional phase steps," *J. Opt. A: Pure Appl. Opt.* **6**, 259–268 (2004).
35. L. Jonathan, Y. Eric, and J. P. Miles, "Observation of the vortex structure of a non-integer vortex beam," *New J. Phys.* **6**, 71 (2004).
36. A. Ambuj, R. Vyas, and S. Singh, "Diffraction of orbital angular momentum carrying optical beams by a circular aperture," *Opt. Lett.* **39**, 5475–5478 (2014).

Biographies for the authors are not available.